JOURNAL OF CATALYSIS 128, 99–112 (1991)

New Supported Palladium–Chromium Catalysts: Characterization and Catalytic Properties

A. BORGNA,[1] B. MORAWECK, J. MASSARDIER, AND A. J. RENOUPREZ[2]

Institut de Recherches sur la Catalyse, 2 Avenue Albert Einstein, F-69626 Villeurbanne, Cédex

Received October 13, 1989; revised September 24, 1990

New silica-supported Pd–Cr catalysts have been prepared either by using mixed inorganic salts of the two metals as precursors or through the deposition of $Cr(CO)_6$ on a monometallic palladium catalyst. Analytic electron microscopy shows that palladium-enriched particles are formed. The EXAFS experiments show that when the reduction temperature reaches 870 K, part of the chromium is reduced and interacts with palladium. In the partial hydrogenation of 1,3-butadiene, these catalysts are less active but 100% selective for the formation of butenes. The explanation, proposed on the basis of hydrogen chemisorption and confirmed by XPS data, is a modification of the electronic structure of palladium, leading to a variation of the adsorption coefficients of the diene and alkenes, compared to the values measured on monometallic palladium catalysts.

INTRODUCTION

The group VIII metals are extensively used in heterogeneous catalysis since they are active in several reactions like hydrogenation, isomerization, hydrogenolysis, oxidation (*1*). Yet, in order to enhance their selectivity and stability, they are frequently promoted with a less noble metal such as Sn, Re, Ge, or Pb (*2, 3*). The preparation of such supported bimetallic catalysts is normally carried out by successive impregnations or by coimpregnations of the two metal salts on an oxide carrier, like SiO_2 and Al_2O_3. The catalyst precursors are subsequently dried and reduced in flowing hydrogen. However, with this method, it is difficult to obtain small bimetallic particles with a homogeneous composition, especially when one of the two metals is difficult to reduce. On the contrary, if the preparation can be performed starting from a mixed salt of the two metals or from heteropolynuclear molecular clusters (*4*) as precursors, the chances of obtaining bimetallic particles with a defined composition may be increased.

Another method of preparation consists of incorporating the second metal in a prereduced monometallic catalyst by sublimation of an organometallic complex, subsequently decomposed in flowing hydrogen (*5*). This method can be advantageous if the second metal is difficult to reduce, since in these complexes the metal atoms are already in the zero oxidation state.

In earlier papers (*6, 7*), we have described the preparation and characterization of Pd–Cr mixed salts and of the bimetallic phase obtained by hydrogen reduction. The aims of this work are (i) to describe the preparation of supported catalysts from these salts and (ii) to compare their structure and reactivity with those of solids obtained by incorporation of chromium by sublimation on a monometallic catalyst.

EXPERIMENTAL

Catalyst Preparation

Supported bimetallic catalysts were prepared by two different methods:

[1] Permanent address: Instituto de Investigaciones en Catálisis y Petroquímica (INCAPE), UNL-CONICET, Santa-Fe, Argentina.

[2] To whom correspondence should be addressed.

0021-9517/91 $3.00

(i) impregnation with an aqueous solution of Pd–Cr mixed salts,

(ii) ion exchange and reduction of Pd, followed by successive $Cr(CO)_6$ sublimation and decomposition.

Impregnation with a mixed salt. The mixed salts, $[Pd(NH_3)_4]Cr_2O_7$ and $[Pd(NH_3)_4]CrO_4$ sources, were prepared as described previously (*6*). After impregnation of the support during 24 h with dilute aqueous solutions of the salts, the solvent was slowly removed in vacuum in a revolving flask at 340 K. Finally, dehydration was completed by drying overnight in a vacuum oven at 370 K. Commercial, nonporous silica (Aerosil 200 Degussa, 130 m^2/g BET specific surface area) has been used as a carrier.

Ion exchange—sublimation. Silica Aerosil 200 was exchanged with a $[Pd(NH_3)_4](OH)_2$ solution followed by air calcination at 670 K and at a low reduction temperature (490 K). After reduction, chromium was incorporated by sublimation of $Cr(CO)_6$ in an oven at 350 K, as described elsewhere (*4*). Finally, the decomposition of the complex was carried out in flowing hydrogen at 470 K.

Catalysts activation. These solids were reduced in flowing hydrogen (1 liter/min) at atmospheric pressure, with a linear temperature rise of 2 K/min, until the final temperature was reached (670 or 870 K). This temperature was maintained for 15 h to favor the interaction between the two metals. Finally, the catalysts were cooled to room temperature under argon before any other experiment. They were never exposed to air before the EXAFS experiments and rereduced at the same temperature before the catalytic activity determination.

Physical Characterization

Small angle X-ray scattering (*SAXS*) experiments were performed on a goniometer equipped with an oven, allowing *in situ* experiments. The pore diameter or particle size distributions were computed as described (*8*), assuming a spherical particle shape. Discrimination between the metal and carrier particles was achieved by a blank experiment using just the support.

EDX-STEM characterization of the catalysts was carried out on a high-resolution VG HB50S scanning microscope, operated at 100 kV and equipped with a Tracor energy dispersive X-ray spectrometer. The analysis was either performed in scanning mode to determine the composition of the whole sample or in spot mode, with a fixed beam, to measure the composition of a given particle.

The concentration ratio of Pd and Cr was computed from the intensities of the Pd$L\alpha$ or Cr$K\alpha$ emission lines, using tabulated normalization factors which take into account the theoretical cross sections, the fluorescence yield, and the efficiency of the detector:

$$C_{Pd}/C_{Cr} = (k_{Pd}/k_{Cr}) \cdot (I_{Pd}/I_{Cr})$$
$$\text{with } k_{Pd}/k_{Cr} = 2.07.$$

Transmission electron microscopy (*TEM*), carried out with a Jeol 100CX instrument, was mainly used to verify that the proportion of large metal particles (60 to 200 Å), barely distinguishable from the silica particles by SAXS, is negligible in our samples. On the silica support, the contrast is high enough to allow a direct observation of the metal particles.

Hydrogen thermodesorption was performed on the samples activated as described above. The samples were outgassed in vacuum at 670 or 870 K before hydrogen admission at 300 K, and were then outgassed at 300 K (10^{-6} Pa) for 2 h (this procedure prevents the formation of a hydride or the presence of physically adsorbed hydrogen). Finally, the thermodesorption experiments were performed by increasing the temperature linearly (30 K/min). The amount of desorbed hydrogen was measured by mass spectrometry (VG micromass) and this quantity was related to the fraction of metal located at the surface, assuming a $H/Pd_S = 1$ stoichiometry, as already discussed (*9*).

EXAFS experiments were performed at

room temperature on the D44 synchrotron beam line (LURE) at both Pd and Cr K-edges. In the latter case, a set of two glass mirrors was inserted between the double-crystal monochromator (Si(311)) and the first ion-chamber, to eliminate higher harmonics. The measurements were made in transmission mode for Pd and in fluorescence mode for Cr. The energy range covered about 800 eV above the edge, with 3-eV intervals at the Pd edge and 2 eV at the Cr edge. The reduced samples (cooled under argon to prevent the formation of hydrides) were transferred under argon in a glove box in sealed containers closed by 40 μm thick Kapton windows. It has been shown elsewhere (*33*) that on similar samples (carbon-supported Pd–Cr catalysts), studied by EXAFS, chromium can be kept in the reduced state in these cells. Only B_1 and S_1 samples reduced at 870 K were studied by X-ray absorption spectroscopy.

The EXAFS signal was extracted from raw data by a conventional procedure (*11*). A linear background was removed from the lower energy part of the absorption coefficient and extrapolated to higher energies. The EXAFS signal was then obtained by fitting a polynomial of increasing degree (n = 2 to 5) in order to determine the atomic-like absorption coefficient, used for normalization of the spectrum. A minimum value of the residual amplitude of the Fourier transform (FT) in the 0- to 1.2-Å range was the criterion for selecting the polynomial degree. Before Fourier transformation, the $k\chi(k)$ signal was multiplied by a Hanning window to reduce the parasitic ripples due to the finite range of the measurement. Typical values for this windowing were: 3–5 $Å^{-1}$ and 12–15 $Å^{-1}$ for the Pd K-edge or 11–14 $Å^{-1}$ for the Cr K-edge, the remaining parts of the spectrum being set to zero. The same type of windowing was applied to compute the inverse FT of a given shell: R_{min} and R_{max} being the extreme values of the R range, the windowing ranges were R_{min}, R_{min} + 0.16 Å and R_{max} − 0.16 Å, R_{max}. All the models have been established by a comparison with the inverse FT of a given shell. In all cases, a reliability factor, Q, was also computed to compare the quality of the various fits (*7*, *14*).

XPS–ESCA and Auger experiments were performed simultaneously on a VG ESCA III instrument (resolution 1 eV–precision 0.15 eV); both signals are excited by the AlK_α radiation. The instrument was equipped with an oven allowing a treatment of the samples under hydrogen up to 900 K before evacuation under 10^{-6} Pa and introduction with a transfer rod in the spectrometer. The Si_{2p} emission of silica, located at 103.4 eV, was used as an internal standard.

Catalytic Reactions

1,3-Butadiene hydrogenation was performed at atmospheric pressure in a flow system equipped with a fixed-bed reactor. The catalysts were reduced *in situ* and the reaction products analyzed by on-line chromatography using an automatic coupling device.

Butadiene hydrogenation was carried out between 280 and 360 K, with $P_{butadiene}$ = 3.9 kPa, $P_{hydrogen}$ = 10 kPa, and He as diluent. In all cases, the conversion was lower than 10%. It was verified by performing the reaction with different mass of catalyst and a large range of gas flow that it is not controlled by a diffusion process. The selectivities S and S_1 in butenes and 1-butene are defined as:

$$S(\%) = 100 \times \Sigma P_{butenes}/(\Sigma P_{butenes} + P_{butane})$$
$$S_1(\%) = 100 \times P_{1\text{-butene}}/\Sigma P_{butenes}$$

and the *trans*-2-butene to *cis*-2-butene ratio as:

$$t/c = P_{trans\text{-2-butene}}/P_{cis\text{-2-butene}}.$$

All these values were taken under steady-state conditions. The competitive benzene-*O*-xylene hydrogenation was performed as described elsewhere (*20*). In this study, which necessitates two separate experiments, the pressure of one of the hydrocarbons was varied between 0.1 and 1 kPa,

TABLE 1

Chemical Analysis Results

Sample	Carrier	Precursor	Pd wt%	Cr wt%	r^a
B_1	SiO_2	Dichromate	0.60	0.58	0.33
C_1	SiO_2	Chromate	0.84	0.44	0.49
S_1	SiO_2	Pd + $Cr(CO)_6$	2.05	0.28	0.78

[a] r: Pd/(Pd + Cr) atomic ratio.

while the pressure of the other was kept fixed. In the meantime, the hydrogen pressure was kept to 10 kPa.

RESULTS AND DISCUSSION

The metallic composition of the catalysts, determined by chemical analysis, is shown in Table 1, together with the Pd/(Pd + Cr) atomic ratio, r. It is significant to note that in the case of the catalysts prepared from mixed salts, the r ratios are in good agreement with the stoichiometry of the precursors (*6*) ($r \approx 0.33$ for dichromate and $r \approx 0.5$ for chromate).

Particle Size Determination

TEM and *in situ* SAXS results are given in Table 2, in which the main peaks of the distribution curves are listed.

The reduction procedure leads to small metallic particles as shown in Figs. 1 and 2. For the low reduction temperature (670 K) the particle size remains similar to that of the standard Pd/SiO_2 catalyst (15 Å) (*10*). Comparison of the curves in Fig. 1, as well as the TEM micrographs of Fig. 2, shows that a slight sintering occurs between 670 and 870 K. However no aggregates larger than 50 Å could be detected on and micrographs. The catalytic activities were therefore calculated with the mean particle size determined by SAXS.

Hydrogen thermodesorption results are given in Table 2. For the B_1 and S_1 catalysts, it was observed that the amount of thermodesorbed hydrogen was appreciably less than that measured on the standard Pd/SiO_2 catalyst which has the same particle size. For example (Table 2), in the case of the catalysts activated at 670 K the n_H/n_{Pd} ratio decreased from 0.60 to 0.15 (B_1 sample) or to 0.18 (S_1 sample). Moreover, this ratio decreased to about 0.05 upon activation at 870 K. This phenomenon may be due either to a reduction of the adsorption capacity by alloying chromium with palladium or to a partial coating of the palladium particles by an oxide phase (*7*).

TABLE 2

Particle Diameter from TEM and SAXS Experiments and Hydrogen Thermodesorption Data

Sample	T_{act}(K)	Particle size(Å)		H_2 thermodesorption n_H/n_{Pd}
		TEM	SAXS	
B_1	670	17	20	0.15
	870	25	28	≈0.05
S_1	670	17	18	0.18
	870	27	28	≈0.05

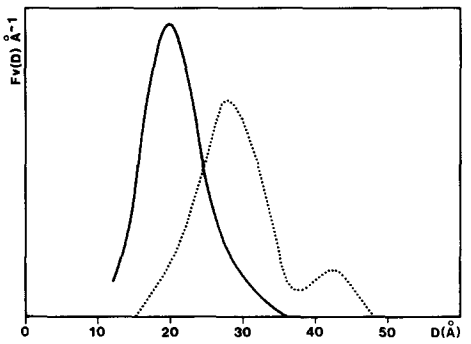

FIG. 1. Particle size distribution obtained by SAXS for sample S_1 reduced at 670 K (solid line) and 870 K (dotted line).

STEM Characterization

This study was only performed on the samples reduced at 870 K. For the B_1 sample, the mean value of the Pd/(Pd + Cr) atomic ratio measured in scanning mode on the whole field is 37 ± 6%, in relatively good agreement with the ratio obtained from chemical analysis (33.5%).

The microanalysis in spot mode of isolated particles has shown that all of them are bimetallic, but with a mean atomic ratio of 71 ± 7%, showing a large increase in the Pd concentration.

Short-Range Order Measured by EXAFS

Pd K-edge. Figure 3a shows the raw EXAFS data for the 15-μm Pd foil used as a reference for the Pd–Pd pairs to extract the experimental amplitude and phase-shift functions (*12*). For the Pd–Cr distance, theoretical values have been used (*13*). The raw EXAFS data at the Pd K-edge for B_1 and S_1 samples are shown in Figs. 3b and 3c.

The curve fitting was first carried out with only Pd atoms as first neighbors. As shown in Figs. 4a and 5a, a relatively good fit is obtained with only Pd–Pd contributions for both samples. Nevertheless, the experimental amplitude is not well represented around 150 eV. From the complete inverse FT it is possible to extract an experimental amplitude function, which constitutes the envelope of the inverse sine transform; this function represents the contribution of the selected shell to the EXAFS signal.

Comparison between the envelope corresponding to the B_1 sample and to that of the standard (Fig. 6) clearly indicates that the surrounding of palladium is different in the catalyst and in the standard, especially around 6 $Å^{-1}$. We have further included Cr atoms in the first coordination shell of Pd. Figures 4b and 5b, as well as the Q values reported in rows 1 and 2 (B_1 sample), 3 and 4 (S_1 sample) of Table 3 show the improvement of the Q factor resulting from the incorporation of Cr atoms in the surrounding of palladium. For both catalysts, it seems that a Pd-enriched Pd–Cr phase is obtained.

Cr K-edge. The same method of data analysis was performed at the Cr K-edge. From the inspection of the FTs (Fig. 7), it is clear that a significant quantity of oxidized chromium is present in the samples. In fact, the first peak can be attributed to Cr–O bonds whereas the assignment of the second one to Cr–metal bonds may be questionable.

We have already shown (*7*) that palladium tetrammine dichromate reduced at 870 K gives rise to an X-ray diffraction pattern which may be unambiguously attributed to a mixture of two phases: the first one (weak and broad lines) corresponds to a metallic phase, the second one (narrow and intense lines) has been indexed as chromium oxide (Cr_2O_3). From the structure proposed by Newnham and de Haan (*15*) for Cr_2O_3, it can be deduced that each chromium atom is surrounded by a distorted octahedron of oxygen atoms located at 1.962(3) and 2.012 Å(3), corresponding to a mean Cr–O distance of 1.987 Å. The second coordination shell is composed of 4 Cr atoms located at 2.645(1) and 2.885 Å(3), giving a mean Cr–Cr distance of 2.825 Å.

Consequently, it clearly appears that the second peak in the FTs, shown in Fig. 7, can be attributed to Cr–Cr distances present in Cr_2O_3. However, this second peak may also be considered as coming from bonds between Pd and Cr, belonging possibly to bimetallic particles. Indeed, alloying two

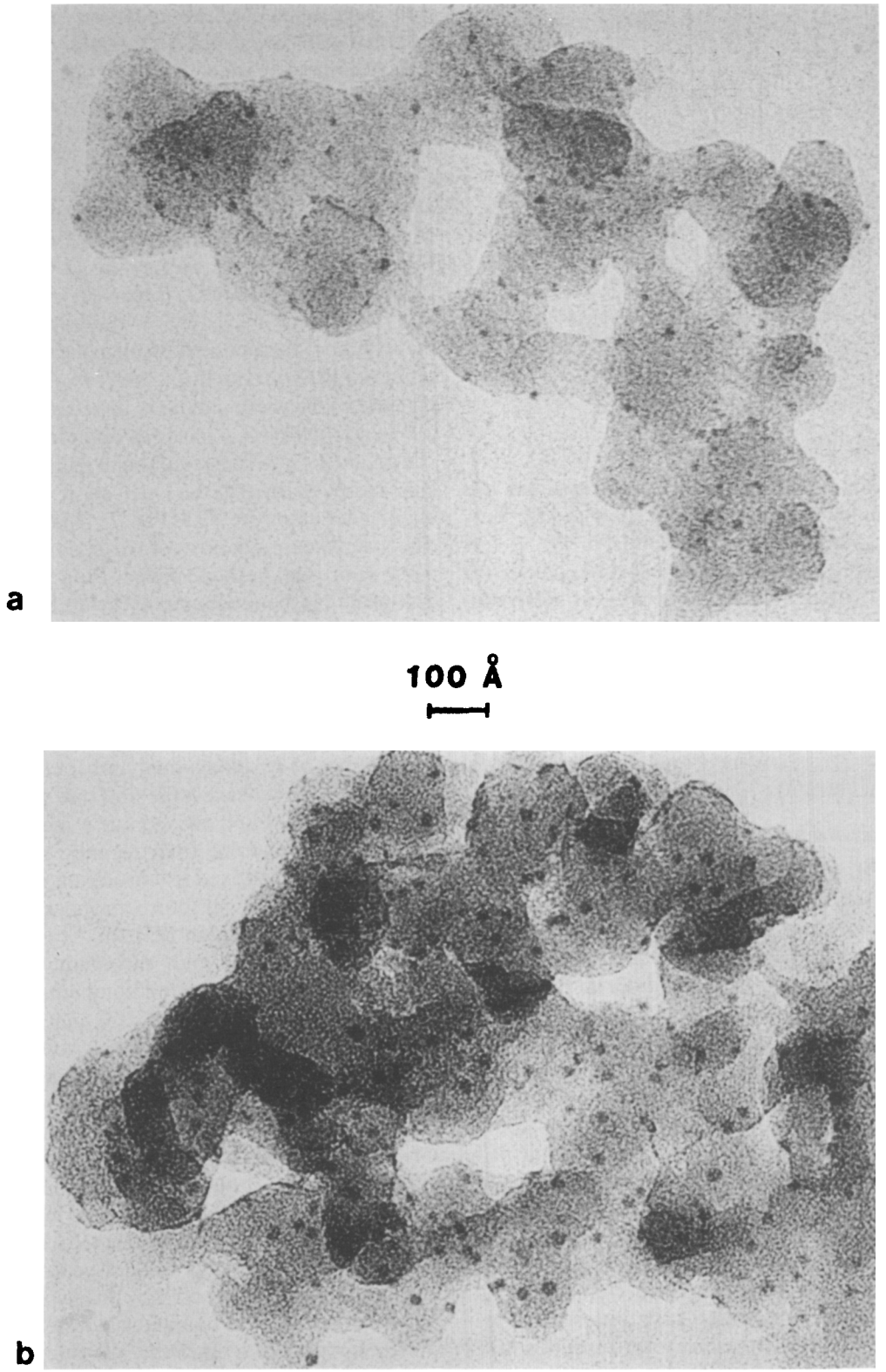

FIG. 2. TEM micrographs for sample S_1 reduced at 670 K (a) and 870 K (b).

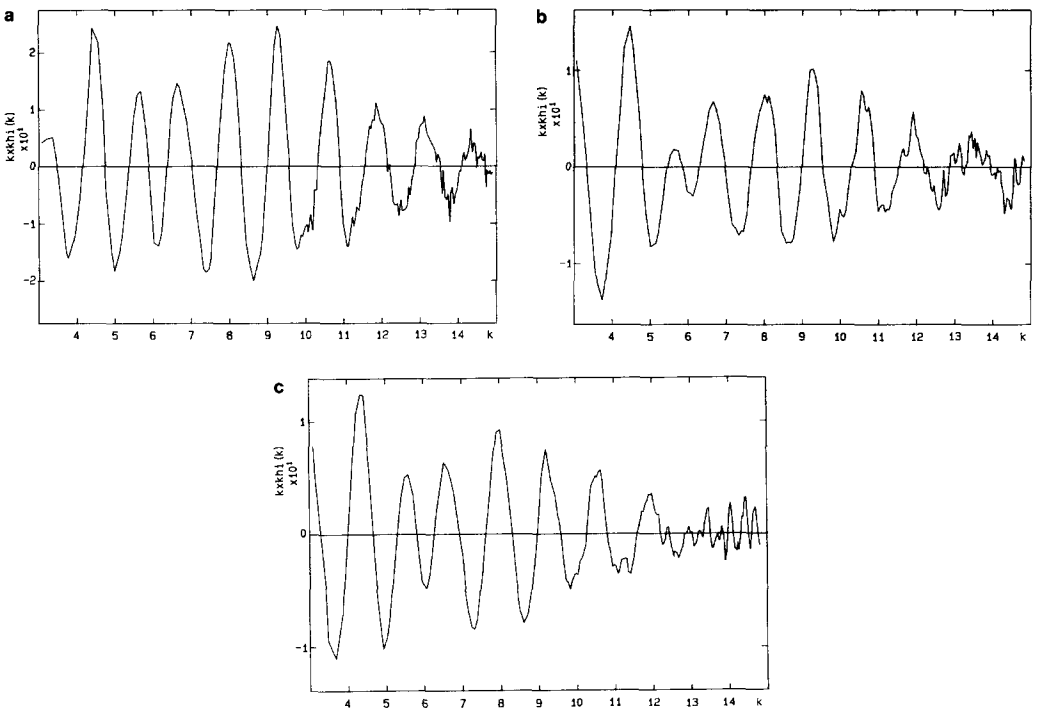

FIG. 3. EXAFS raw data at the Pd K-edge: (a) Pd 15 μm foil, (b) B_1 sample, (c) S_1 sample.

metals such as Pd and Cr leads to nearest Pd–Cr distances in the range 2.75 Å (bulk Pd)–2.50 Å (bulk Cr). A Pd–Cr distance in a bimetallic Pd–Cr phase will be about 0.1 Å smaller than a Cr–Cr distance in Cr_2O_3. Moreover, if both types of distances contribute to the EXAFS signal, they can be identified because of the important difference between Pd and Cr backscattering amplitudes. Tables 4 and 5 and Fig. 8 report the result of a complete analysis of EXAFS data for sample B_1.

We have first tried to model the whole FT, assuming that the two main peaks could

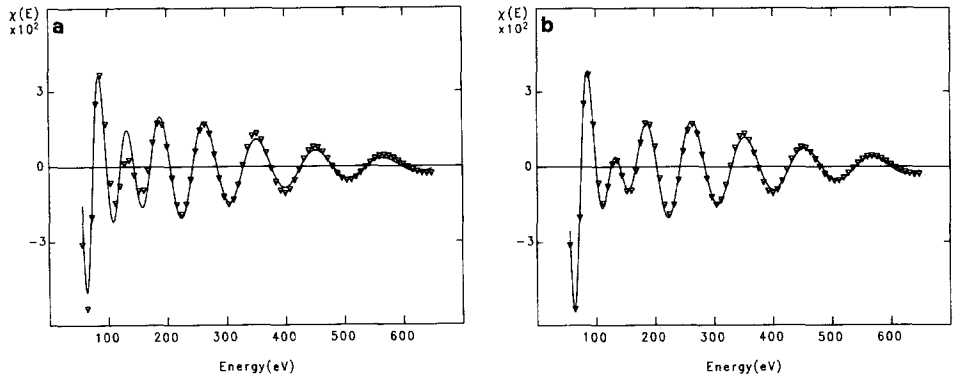

FIG. 4. EXAFS at the Pd K-edge for sample B_1 reduced at 870 K: (a) fit without Cr atoms, (b) fit with Cr atoms introduced in the first coordination shell of palladium.

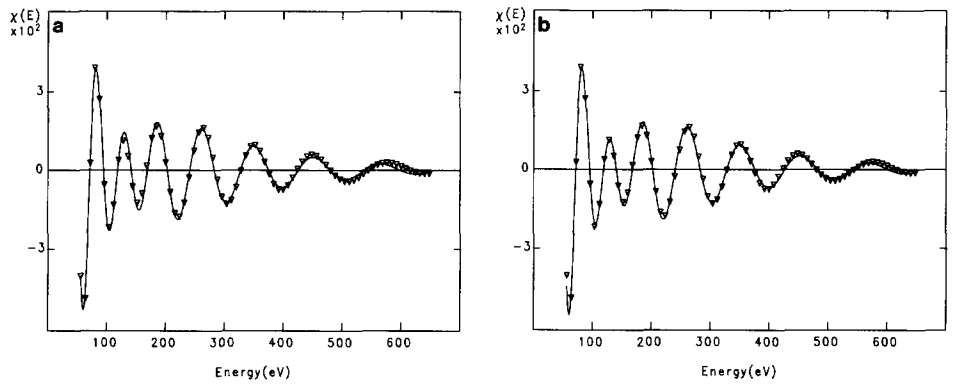

FIG. 5. EXAFS at the Pd K-edge for sample S_1 reduced at 870 K: (a) fit without Cr atoms, (b) fit with Cr atoms introduced in the first coordination shell of palladium.

be treated as a mixture of Cr–O, Cr–Cr and Cr–Pd pairs. The results concerning this model are summarized in Fig. 8 and Table 4. A good fit between experimental and calculated spectra is obtained, leading to the following conclusions: two phases are present in this catalyst; the first one is an oxide, Cr_2O_3, with a Cr–O distance of 2.03 Å, close to the mean value of 1.987 Å in bulk Cr_2O_3. The second coordination shell is composed of Cr atoms located at 2.80 Å, a distance slightly smaller than the Cr–Cr distance in Cr_2O_3, together with a Cr–Pd contribution involving 1.0 Pd atom at 2.73 Å.

The coordination numbers of 1.4 Cr and 4.5 O, as well as the lack of well-defined peak beyond 2.8 Å in the FT, suggest that the Cr_2O_3 particles on the carrier surface display no longrange order and are quasi-amorphous.

Nevertheless, one cannot exclude that part of this "oxide" phase may be in relatively close interaction with the metal. This second phase which is evidenced by the model at the Cr K-edge as well as at the Pd K-edge, may be ascribed to a bimetallic phase, largely palladium-enriched compared to the chemical composition of the precursor.

To corroborate these conclusions, two other models may be built upon the second peak of the FT only. This was done by assuming either only Cr–Cr distances belonging to the oxide phase or a mixture of Cr–Cr and Cr–Pd pairs. The results of the first model are illustrated on Fig. 9a; obviously, it does not describe correctly the second coordination shell of chromium, which is reflected by the very large value of the reliability factor Q (Table 5). Conversely, the second model (Fig. 9b) leads to a good fit (Q = 0.07). More important is that, as in the case of the model built on the whole EXAFS spectrum, the coordination number and the Cr–Pd distance (always optimized in the computing process), are in complete agreement with the corresponding values determined at the Pd K-edge.

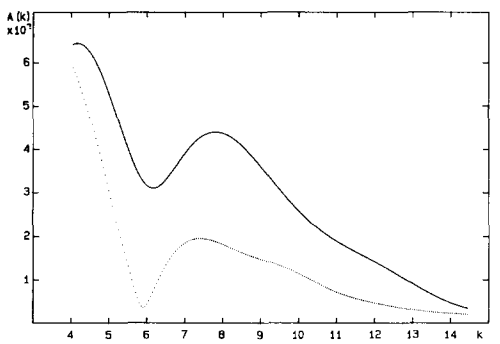

FIG. 6. Comparison between amplitude envelopes for sample B_1 (dotted line) and standard Pd foil (full line).

TABLE 3

EXAFS Results at the Pd K-Edge

Catalyst	Bond	Coord. no.	R(Å)	$\sigma \times 10^{-2}$(Å)	Q
B_1[a]	Pd–Pd	8.03	2.75	5.519	0.264
B_1	Pd–Pd	8.97	2.78	5.697	0.106
	Pd–Cr	0.72	2.73	0.351	
S_1[a]	Pd–Pd	8.38	2.76	6.654	0.114
S_1	Pd–Pd	8.82	2.77	7.063	0.089
	Pd–Cr	0.17	2.69	0.107	

[a] Only if Pd atoms are considered in the first coordination shell.

Consequently it can be deduced that:

(i) Most of the chromium is in interaction with oxygen atoms, under the form of oxide (Cr_2O_3) (*7*) or via chromium-support interaction. This conclusion appears specially valid for the catalyst prepared from mixed salts.

(ii) The comparison between EXAFS experiments and STEM data shows that only a fraction of chromium is reduced and is in close interaction with palladium for the B_1 and S_1 samples reduced at 870 K.

(iii) The total mean coordination number of palladium, 9 to 10.5 measured by EXAFS, is in agreement with the particle size (20–25 Å) determined by TEM or SAXS.

Electronic Structure Modifications

To verify the existence of possible electronic structure modifications of palladium, XPS experiments were performed on Pd/SiO_2 and various Pd–Cr/SiO_2 catalysts. The bimetallic catalysts were reduced *in situ* at 870 K in flowing hydrogen and introduced after evacuation, with the transfer rod, in the ESCA machine.

The interpretations of core-level binding energy shifts (δE_b) measured by XPS, on small metal aggregates deposited on various substrates, have been reviewed by Mason (*16*). Moreover, he has shown that alloying a noble metal can produce a similar shift of the binding energy measured by XPS to that observed upon increasing the cluster size. Early works on small aggregates, reporting the observations of core-level shifts, were interpreted as resulting from a size depen-

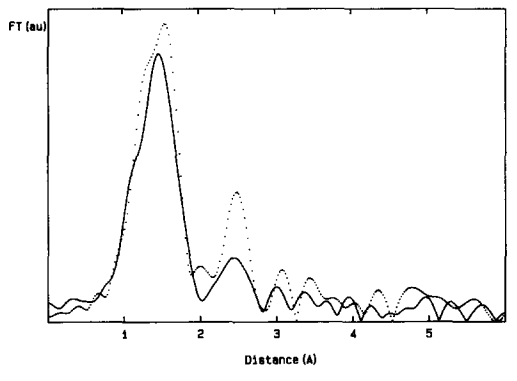

FIG. 7. EXAFS radial distribution function at the Cr K-edge for sample S_1 (solid line) and sample B_1 (dotted line), obtained by k^3-weighted FT.

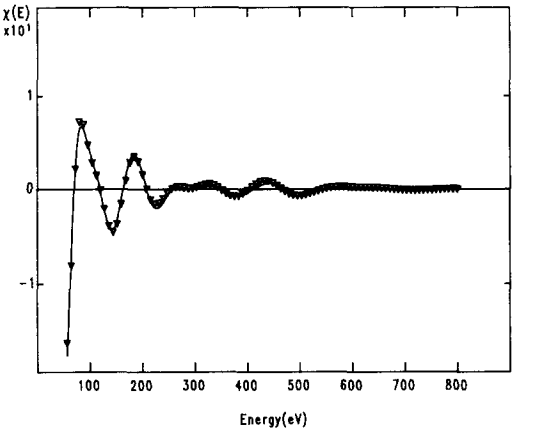

FIG. 8. Curve fitting at the Cr K-edge: fit on the whole spectrum.

TABLE 4

EXAFS Results at the Cr K-Edge (Whole Spectrum) for B_1 Sample

Bond	Coord. no.	R(Å)	$\sigma \times 10^{-2}$(Å)	Q
Cr–O	2.6	2.03	5.0	0.072
Cr–Cr	1.4	2.80	5.0	
Cr–Pd	1.0	2.73	0.4	

dence of the initial-state electronic structure. A later work (*17*) concluded that the shifts are due rather to variations in the final-state relaxation processes. Actually, the conclusions of Mason are that metallic clusters deposited on insulators such as SiO_2 show upward shifts of the order of 1 eV when the mean coordination number decreases from 12 in bulk Pd to 2–3 in the smallest clusters. On the basis of the model developed by Bahl *et al.* (*18*), the contribution to this shift ascribable to extra-atomic relaxation energies, δR_{ex}, can be evaluated. A combination of the measured Auger M_{5VV} and XPS Pd $3d^{5/2}$ emissions, which are both excited by the AlK_α radiation, was used by these authors, who have shown that δR_{ex} has the expression

$$\delta R_{ex} = (\delta E_k + \delta E_b)/2,$$

where δE_k and δE_b are respectively the Auger and XPS line shifts with respect to the bulk Pd reference sample. It can be seen in Table 6 that δR_{ex} does not exceed -0.25 ± 0.05 eV. The cluster size and thus δR_{ex} is not appreciably changed by the addition of a small amount of Cr in the Pd particles. Thus, the downward orbital energy shifts, $\delta E_s = \delta E_b + \delta R_{ex}$, measured on the B_1 and S_1 samples, are 0.95 and 0.75 eV.

In the work reported by Mason (*16*) concerning the shifts of E_b (Au $4f_{7/2}$) observed upon alloying gold with nickel, palladium, etc., it is stated that this metal could maintain near neutrality and only undergo a rehybridization. In the present case, alloying Pd with Cr may also only induce a rehybridization between the 4*d* and 4*s* levels of palladium.

The same trends are deduced from the observed modifications of the Pd K-edge of the B_1 catalyst. It is clear from Fig. 10 that

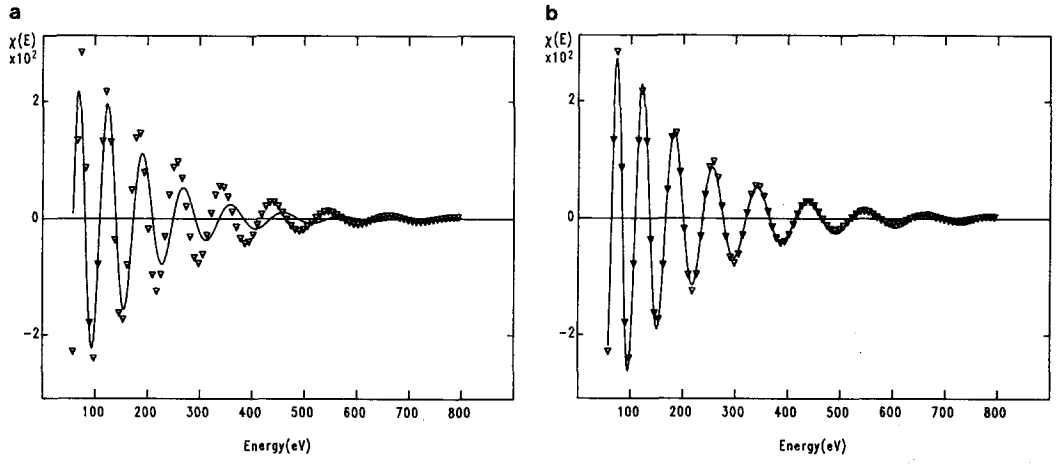

FIG. 9. Curve fitting at the Cr K-edge: fit of the second peak of the FT. Considering the attribution of this peak, (a) to Cr–Cr distances in the oxide phase and (b), to Cr–Cr and Cr–Pd distances.

TABLE 5

EXAFS Results at the Cr K-Edge (Second Peak) for B_1 Sample

Bond	Coord. no.	R(Å)	$\sigma \times 10^{-2}$(Å)	Q
Cr–Cr	2.6	2.85	9.0	0.480
Cr–Cr	1.6	2.82	5.5	0.071
Cr–Pd	0.95	2.73	0.5	

even the presence of a very small amount of Cr in the neighborhood of Pd modifies the edge structure. A flattening of the structure attributed to the $1s \rightarrow 4d,5s$ transition is observed. This modification also constitutes an indication of a transfer of charge to the Pd $4d$ band produced by the presence of Cr atoms in the Pd particles. A similar effect has been already observed in Pt–Fe/charcoal catalysts (*19*) for which it has been shown that an oxidizable metal such as Fe tends to induce an increase of the density of states in the Pt $5d$ band, resulting in a decrease of the white line at the Pt L_{III}-edge. An opposite and simultaneous effect is observed at the Fe K-edge, which exhibits an increase of the $1s \rightarrow 3d,4s,4p$ features.

Unfortunately, in the case of our Pd–Cr catalysts, this effect is completely hidden by the presence of a white line, originating from the presence of an important quantity of chromium oxide, as demonstrated by the EXAFS experiments at the Cr K-edge.

In order to ascertain this conclusion, competitive hydrogenation between benzene (Bz) and *ortho*-xylene (oxyl) was carried out. The adsorption coefficients ratio, b_{oxyl}/b_{Bz}, between benzene and *ortho*-xylene was determined. On Pd samples, this ratio, 22.5, is higher than that on Pd–Cr catalysts, 17. This would mean that the density of states of palladium, near the Fermi level, is increased by the presence of chromium (*20*).

Reactivity of the Pd–Cr-Supported Catalysts

The effect of chromium on the reactivity of palladium in the 1,3-butadiene hydrogenation has been investigated. This reaction was chosen because of its relatively well-known mechanism (*21–23*). A rake-like scheme is generally proposed to explain the selectivity for partial hydrogenation and the distribution of the various butenes.

The reaction would occur through the following pathway:

$$\begin{array}{ccccc} C_4H_6(g) & & C_4H_8(g) & & \\ \downarrow\uparrow & & \downarrow\uparrow & & \\ C_4H_6(ad) & \xrightarrow{+H_2} & C_4H_8(ad) & \xrightarrow{+H_2} & C_4H_{10}(g) \end{array}$$

According to this scheme, the selectivity depends both on the relative hydrogenation rates and on the relative adsorption strengths between the diene and the intermediary olefins.

The results obtained with the different Pd–Cr catalysts are shown in Table 7. A standard Pd/SiO_2 catalyst is also included

TABLE 6

XPS Data on Bulk Pd and Supported Pd and Pd–Cr Catalysts

Sample	d(Å)	E_b $3d^{5/2}$(eV)	δR_{ex} (eV)	δE_s (eV)
Pd(111)		335.6	0.0	0.0
Pd/SiO_2	17	335.6	−0.25	−0.25
B_1	27	334.9	−0.25	−0.95
S_1	27	335.1	−0.25	−0.75

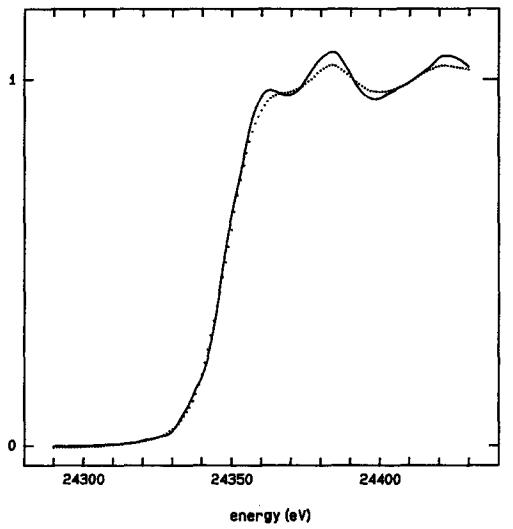

FIG. 10. Pd near edge structure for standard foil (full line) and sample B_1 (dotted line).

as a reference. It is significant to remark that the turnover numbers quoted in Table 7 were calculated with the mean particle diameters given by SAXS. In all cases, the addition of chromiun increases the selectivity for partial hydrogenation and decreases the catalytic activity (4–20 times).

The explanation of these phenomena may be ascribed to both electronic and geometric factors, the relative importance of which has been already discussed (*24*). A first assumption would be that the decrease of activity and of hydrogen adsorption capacity can be attributed to a geometric effect. In our case the geometric effect may be due to a dilution effect either by the chromium atoms located at the surface of the particles and/or by the partial coating of the surface by chromium oxide. If this second assumption is plausible for catalysts prepared from mixed salts, especially for sample B_1, composed of particles containing 30% chromium as shown by STEM, it must be discarded for sample S_1 containing only a small amount of chromium.

Moreover, the activity decrease has also been frequently related to metallic dispersion. However, in our case practically the same particle size has been observed for the Pd–Cr catalysts reduced at 670 K, (18 Å) and for the standard Pd/SiO_2. Consequently, a particle size variation cannot wholly account for the decrease of catalytic activity.

A geometric effect cannot explain (i) the relative increase of activity observed when the reduction temperature is increased from 670 to 870 K on sample S_1 and C_1, whereas the hydrogen adsorption capacity is strongly decreased; (ii) the enhancement of selectivity (98–100% compared to 90), for all the samples containing chromium. The observed modification of the electronic structure of palladium is thus certainly involved.

Such a modification of selectivity induced by an electronic effect has been already reported in the literature. Recently, Boitiaux *et al.* (*25, 26*) studying the influence of electron-donating and -attracting compounds in

TABLE 7

Reactivity for the Hydrogenation of 1,3-Butadiene

Sample	T_{act}(K)	$n(s^{-1})$	S(%)	S1(%)	t/c
B_1	670	0.11	99.4	—	—
	870	0.10	100.0	—	—
C_1	670	0.11	97.6	52.0	2.04
	870	0.20	98.8	46.0	2.63
S_1	670	0.28	97.8	48.0	1.78
	870	0.48	100.0	52.0	3.84
Pd/SiO_2	670	1–2.00	90.0	60.0	1.86

the hydrogenation of 1,3-butadiene and 1-butyne, showed that the two kinds of compounds have an opposite effect, which excludes a geometric explanation. Their results were interpreted by a modification of the metal-unsaturated hydrocarbon interaction induced by ligand-effect. Okamoto *et al.* (*27*) have shown a similar correlation between the butene distribution and the electronic density of Ni metal.

The change in selectivity is qualitatively explained taking into account the volcano curve reported by Boitiaux *et al.* (*28*), when the actual rate constants for the hydrogenation reactions are plotted against the adsorption constants of these hydrocarbons. Thus, a modification of the metal electronic structure would induce a change of selectivity, since the adsorption constants of hydrocarbons are affected differently. In a previous paper (*29*), it was shown, by means of the study of the competitive butadiene–butene hydrogenation, that the greater selectivity on palladium compared to platinum can be attributed to its capacity of adsorbing more strongly a diene than an alkene molecule. Therefore, our results suggest that electronic factors must be invoked to explain the effect of chromium addition on the selectivity.

Moreover, in relation to the modifications of the active sites induced by the Cr addition, it may be noted that the apparent activation energy is 42 $kJ.mol^{-1}$ on Pd–Cr samples and only 35 $kJ.mol^{-1}$ on Pd samples, which could result in the weakening of the H_2 adsorption strength on the bimetallic catalysts. This increase of density of states in the 4*d* band of palladium induced by chromium would act as an electron-donor like piperidine in the work of Boitiaux *et al.* (*30*), increasing the selectivity toward butenes.

Simultaneously with the increase of partial hydrogenation selectivity, the distribution of butenes is also slightly altered. The selectivity for the formation of 1-butene, S_1 (46–52%), is slightly lower than that on the monometallic reference catalyst (60%).

Such a decrease of S_1 and the corresponding increase of *trans*-/*cis*-2-butene ratio when the S selectivity increases, has also been observed by Boitiaux *et al.* (*30*), upon addition of piperidine.

Nevertheless, despite this electronic structure modification and its consequence on the volcano curve already discussed, an increase of activity is expected, which has not been observed. The reason could be an important deactivation caused by oligomerization reactions favored by the presence of chromium oxide (*32*) on these catalysts, the amount of which is lower in the samples reduced at high temperature.

CONCLUSION

Starting from mixed salts, palladium dichromate, or chromate, or $Cr(CO)_6$ sublimated on a preduced Pd/SiO_2 catalyst, well-dispersed silica-supported Pd–Cr catalysts were obtained, showing an uniform distribution of the metal particles on the support. The combination of STEM and EXAFS data has shown that the particles are palladium enriched compared to the precursors. On the other hand, only 10 to 25% of the chromium is in the metallic state; the remaining part is neighboring or at the surface of the particles, under the form of oxide. The Cr^0/Cr^{3+} ratio could be dependent both on the preparation mode and on the reduction temperature.

In the hydrogenation of 1,3-butadiene, the supported Pd–Cr samples are fully selective for the partial hydrogenation, whereas the corresponding Pd/SiO_2 is only 90% selective. This enhancement of selectivity is well explained by a rehybridization of palladium on the effect of chromium, which increases the ratio of the adsorption constant of butadiene with respect to that of butenes.

The observed reduction of activity of the bimetallic samples is explained by the oligomerization of the diene on chromium oxide inducing a stronger deactivation.

As can be expected from the results obtained with the lowest chromium concentration sample, one may hope that an optimum Pd/Cr ratio can be reached to obtain a 100% selectivity without any activity reduction.

ACKNOWLEDGMENTS

We thank M. T. Gimenez, F. Bauchesne, C. Nicot, and G. Clugnet for their technical assistance, and the LURE staff for dedicated runs. We are also grateful to P. Fessler for help during EXAFS experiments. One of us (A.B.) is indebted to CNRS and CONICET for financial support.

REFERENCES

1. Rylander, P. N., "Hydrogenation Methods." Academic Press, London, 1985.
2. Yermakov, Y. I., *React. Kinet. Catal.* **14,** 99 (1980).
3. Travers, C., Bournonville, J. P., and Martino, G., "Proceedings, 8th International Congress on Catalysis, Berlin, 1984," Vol. 4, p. 891. Dechema, Frankfurt-am-Main, 1984.
4. Choplin, A., Huang, L., Theolier, A., Gallezot, P., Basset, J. M., Siriwardane, U., Shore, S. G., and Mathieu, R., *J. Amer. Chem. Soc.* **108,** 4224 (1986).
5. Borgna, A., Thesis, U.N.L., Santa Fe, 1987.
6. Borgna, A., Moraweck, B., and Fessler, P., *Powder Diffract.* **4,** 217 (1989).
7. Borgna, A., Moraweck, B., and Renouprez, A. J., *J. Chim. Phys.* **86,** 1719 (1989).
8. Renouprez, A. J., Hoang Van, C., and Compagnon, P. A., *J. Catal.* **34,** 411 (1974).
9. Moraweck, B., Clugnet, G., and Renouprez, A. J., *J. Chim. Phys.* **83,** 265 (1986).
10. Ouchaib, T., Thesis, Université Claude Bernard, Lyon, 1989.
11. Moraweck, B., and Renouprez, A. J., *Surf. Sci.* **106,** 35 (1981).
12. Lee, P. A., Citrin, P. H., Eisenberger, P., and Kincaid, B. M., *Rev. Mod. Phys.* **53,** 769 (1981).
13. Teo, B. K., and Lee, P., *J. Amer. Chem. Soc.,* **101,** 2815 (1979).
14. Schwartz, L. H., and Cohen, J. B., "Diffraction from Materials," p. 295. Academic Press, New York, 1977.
15. Newnham R. E., and de Haan, Y. M., *Z. Kristallogr.* **117,** 235 (1962).
16. Mason, M. G., *Phys. Rev. B* **27,** 748 (1983).
17. Kohik, S., *Appl. Surf. Sci.* **25,** 81 (1986).
18. Bahl, M. K., Tsai, S. C., and Chung, S. C., *Phys. Rev. B* **21,** 1344 (1980).
19. Moraweck, B., Bondot, P., Goupil, D., Fouilloux, P., and Renouprez, A., *J. Phys. Paris C8* **48,** 297 (1986).
20. Phuong, T. T., Massardier, J., and Gallezot, P., *J. Catal.* **102,** 456 (1986).
21. Bond, G. C., Webb, G., Wells, P. B., and Winterbottom, J. M., *J. Chem. Soc.,* 3218 (1965).
22. Wells, P. B., and Bates, A. J., *J. Chem. Soc (A),* 3064 (1968).
23. Phillipson, J. J., Wells, P. B., and Wilson, G. R., *J. Chem. Soc. (A),* 1351 (1969).
24. Sachtler, W. M. H., *Catal. Rev. Sci. Eng.* **14,** 193 (1976).
25. Boitiaux, J. P., Cosyns, J. P., and Robert, E., *Appl. Catal.* **49,** 219 (1989).
26. Boitiaux, J. P., Cosyns, J. P., and Robert, E., *Appl. Catal.* **49,** 235 (1989).
27. Okamoto, Y., Fukino, K., Imanoka, T., and Teranishi, S., *J. Catal.* **74,** 173 (1982).
28. Boitiaux, J. P., Cosyns, J. P., and Robert, E., *Appl. Catal.* **32,** 169 (1987).
29. Ouchaib, T., Massardier, J., and Renouprez, A. J., *J. Catal.* **119,** L517 (1989).
30. Boitiaux, J. P., Cosyns, J., and Robert, E., *Appl. Catal.* **35,** 193 (1987).
31. Smith, L. B., and Massintil, J. L., *J. Amer. Chem. Soc.* **83,** 4301 (1961).
32. Jozwiak, W. J., Dalla Lana, I. G., Przystajko, W., and Fiederov, R., "Proceedings, 9th International Congress on Catalysis, Calgary, 1988" (M. J. Phillips and M. Ternan, Eds.), Vol. 3, p. 1340. Chem. Institute of Canada, Ottawa.
33. Ouchaib, T., Moraweck, B., Massardier, J. and Renouprez A., *Catal. Today* **7,** 191 (1990).